

RNA export factor RAE1 contributes to NUP98-HOXA9-mediated leukemogenesis

メタデータ	言語: eng 出版者: 公開日: 2017-10-06 キーワード (Ja): キーワード (En): 作成者: メールアドレス: 所属:
URL	https://doi.org/10.24517/00039997

This work is licensed under a Creative Commons Attribution-NonCommercial-ShareAlike 3.0 International License.



RNA export factor RAE1 contributes to NUP98-HOXA9-mediated leukemogenesis

Tatsuyoshi Funasaka^{1*}, Hiroshi Nakano^{1,8*}, Yu Wu^{2,3*}, Chieko Hashizume¹, Ling Gu⁴, Takuro Nakamura⁵, Wei Wang^{1,8}, Pengbo Zhou⁶, Malcolm AS Moore⁷, Hiroshi Sato⁸ and Richard W.Wong¹

1 Frontier Science Organization and Cancer Research Institute, Kanazawa University, Kakuma-machi, Kanazawa, Ishikawa 920-1192, Japan.

2 Department of Hematology and Hematology Research Laboratory, State Key Laboratory of Biotherapy and Cancer Center, West China Hospital, Chengdu, China.

3 Laboratory of Genome Stability, Development and Stem Cell Institute, West China Second University Hospital, Sichuan University, Chengdu, China.

4 Laboratory of Hematology, Department of Pediatric Hematology, West China Second University Hospital, Sichuan University, Chengdu, China

5 Department of Carcinogenesis, The Cancer Institute, Tokyo, Japan.

6 Department of Pathology and Laboratory Medicine, Weill Medical College and Graduate School of Medical Sciences of Cornell University, New York, New York 10065, USA.

7 Cell Biology Program, Memorial Sloan-Kettering Cancer Center, New York, NY 10065, USA.

8 Department of Molecular Virology and Oncology, Cancer Research Institute, Kanazawa University, Kanazawa, Japan.

* These authors contributed equally.

Corresponding author:

Dr. Richard Wong

Frontier Science Organization, 1/F Cancer Research Institute,

Kanazawa University, Kakuma-machi, Kanazawa, Ishikawa 920-1192 Japan.

Tel: +81-76-264-6716; Fax: +81-76-234-4510.

E-mail: rwong@staff.kanazawa-u.ac.jp

Abstract

Chromosomal translocations involving chimeric fusions of the nucleoporin NUP98 protein have often been described in acute myelogenous leukemia (AML). All the fusion proteins have an identical NUP98 N-terminus, which contains the GLEBS motif for interaction with the mRNA export factor RAE1, and FG repeats that associate with the transcription factors HDAC1 and p300. It is virtually unknown whether these interaction partners affect leukemogenesis. We previously showed that RAE1 depletion caused aneuploidy, which enhanced tumorigenesis. We speculated that RAE1 may also be directly involved in NUP98 fusion-mediated leukemogenesis. We show here that RNA interference (RNAi)-mediated knockdown of NUP98 caused severe chromosome segregation defects and disrupted RAE1 but not HDAC1 expression and localization. Next, we performed rescue experiments to confirm that the RAE1-NUP98 complex orchestrates proper chromosome segregation. Interestingly, we found diverse behaviors of NUP98 and the leukemogenic fusion protein NUP98-HOXA9 throughout the cell cycle. Strikingly, in NUP98-HOXA9-transfected cells, RAE1 protein were reduced and mis-localized. Our cellular interpretations were further confirmed by NUP98-HOXA9 transgenic mice and the NUP98-HOXA9 AML patient. These data suggest that RAE1 orchestrates NUP98-mediated leukemogenesis and raise the possibility that targeting

this negative feedback loop may provide a new strategy for the therapy of aggressive leukaemias.

Introduction

The nuclear pore complex (NPC) is composed of at least 30 different nucleoporins act as gatekeeper regulating transport between the cytoplasmic and nuclear compartments [1-5]. One of them, termed NUP98, which located on the chromosome 11p15 have been repeatedly implicated in AML, chronic myelogenous leukemia, T-acute lymphocytic leukemia and in myelodysplastic syndrome (MDS) [6-8]. Over twenty genes have been reported as fusion partners of NUP98 in patients with leukemia [6]. All the disease-associated translocations involving *NUP98* result in the fusion of the 5' end of *NUP98* to the 3' end of a partner gene. The fusion proteins that arise juxtapose the N-terminal FG (phenylalanine-glycine) repeats of NUP98, the presumed contact sites for another nucleoporin, RNA export factor 1 homolog (*S. pombe*) (RAE1) [9-12] and for the transcription factors histone deacetylase 1 (HDAC1) and CREB binding protein CBP/p300, to the C-terminus of the partner protein [13]. NUP98 fusions identified in patients frequently involve homeodomain transcription factors, most commonly HOXA9 [13]. NUP98-HOXA9 consists of amino acids 1–469 of NUP98 joined to amino acids 163–271 of HOXA9; chimeric fusion proteins retain the C-terminal sequence of the transcription factor, including the 60-amino-acid homeobox, which is responsible for binding DNA [14]. Moreover, the NUP98-HOXA9 translocation has been frequently observed in Asians, and the prognosis of patients with this aberration is poor [13, 14].

A general cellular model for NUP98-homeodomain fusion-induced leukemogenesis cites aberrant transcriptional activation of novel target genes as the basis for cellular transformation [13, 15], but there is insufficient direct clinical evidence for this hypothesis [6-8, 16]. On the other hand, RAE1, a *bona fide* binding partner of NUP98

[17, 18], has been indicated as abnormal in breast [19, 20] and lung [21] cancer patients. We and others demonstrated that RAE1 is critical in the maintenance of spindle bipolarity: depleted RAE1 leading to chromosome instability and multipolar spindles, caused aneuploidy, which is often found in various cancers [10-12, 22]. An attractive possibility for NUP98 fusion-mediated leukemogenesis is that functional RAE1 is reduced in NUP98 leukemogenic fusion cells. This would enhance supernumerous spindle pole formation/multiple centrosomes, which would enhance tumorigenesis. This aspect of NUP98-mediated leukemogenesis has not been explored at all.

Results

RAE1 and NUP98 is involved in regulating proper chromosome segregation to prevent aneuploidy formation

Before testing our hypothesis that RAE1 may contribute to NUP98-HOXA9 leukemogenesis, we first tested whether altering endogenous NUP98 levels would affect RAE1 localization and expression, using knockdown by small interfering RNA (siRNA). Quantitative immunoblot analysis of HeLa cells subjected to *NUP98* siRNA treatment for 72 h revealed a ~75% reduction in NUP98 compared with control cells ($p < 0.05$) (Figure 1A, upper panel). In siRNA-mediated *NUP98*-knockdown HeLa cells, we found that RAE1 protein levels were decreased by 70%, whereas the amounts of other nucleoporins (Tpr and p62) or HDAC1 (Figure 1A, B and Supplementary information, Figure S1A-C) and tubulin (as a loading control) were largely unaltered (Figure 1A). Furthermore, identical results were obtained in two leukemia cell lines (K562 and KG1) (Supplementary information, Figure S1D-G). To confirm that the observed reduction in the expression of RAE1 was not artifactual, and to assess RAE1 localization in NUP98-depleted HeLa cells, we performed immunostaining using antibodies against NUP98 and RAE1 in interphase cells. Notably, depletion of NUP98 abolished the expression and localization of RAE1 at the nuclear rim during interphase (Figure 1C, indicated by a white circle), in contrast to the NUP98 and RAE1 endogenous expression pattern observed with control siRNA (Figure 1C, upper panel). Using DAPI staining to monitor nuclear/chromatin alterations, we found that the frequency of “small-nuclei” (sized were 30% reduced compared with WT) was increased by 27% ($n > 300$ mitotic cells) in NUP98-depleted cells (Figure 1C). To test this “small-nuclei” notion further, we performed live cell imaging of *NUP98* siRNA, control siRNA, or siRNA for another

nucleoporin, translocated promoter region (*TPR*), transfected into green fluorescent protein-histone H2B (GFP-H2B) stable cell lines. Abnormal nuclear/chromatin phenotypes were easy to observe in *NUP98* siRNA GFP-H2B cell lines ([Supplementary information, Figure S2B](#)), but the same phenotypes were rarely found in control siRNA or *TPR* siRNA-transfected cells ([Supplementary information, Figure S2A and C](#)). Thus, these alterations in nuclear architecture likely reflect a role for NUP98 directly in forming nuclei or in influencing chromosomal dynamics during mitosis; deregulation of the latter process has previously been found to result in a very similar nuclear appearance [23, 24]. These data prompted us to speculate that NUP98 might contribute to chromatin/histone modifications; however, we did not find any change in the localization or expression of HDAC1, which binds NUP98 in the chromatin, in our routine protocols ([Supplementary information, Figure S1H](#)).

We next sought to determine the consequences of NUP98 depletion on RAE1 localization during mitosis. Interestingly, when NUP98 knockdown was incomplete, some RAE1 remained localized at the kinetochores and spindles ([Figure 1D](#), white arrows) and most of the cells were bipolar with single rod-shaped chromosomes (by DAPI staining). On the other hand, in cells in which NUP98 was almost entirely depleted, RAE1 localization was abolished from kinetochores and spindles, and remarkable chromosome separation defects were found in 22% ([Figure 1E](#)). Particularly, *NUP98* siRNA treatment of mitotic cells was consistently associated with abnormal congression of chromosomes at the metaphase plate. More than 22% of HeLa cells showed separation defects, whereas these defects were not found in control siRNA-treated cells ([Figure 1 D and E](#), white circle). The reduction of NUP98 by RNAi

also led to the formation of multipolar spindles. We quantified the mitotic defects 72 h after transfection with siRNA targeting *NUP98* and found that a high proportion (~30%) of cells displayed strikingly altered spindle morphology compared with control siRNA-transfected cells ($n > 300$ mitotic cells) (Figure 1E, F and Supplementary information, Figure S3). To investigate the chromosome separation defects further, we performed live cell imaging of *NUP98* siRNA or control siRNA transfected into GFP-tubulin or GFP-H2B stable cell lines. Defective chromosome phenotypes in *NUP98* siRNA GFP-H2B cells (Supplementary information, Figure S4B), and multipolar spindles in *NUP98* siRNA GFP-tubulin cells (Supplementary information, Figure S4D), were clearly observable; however, they were rarely found during live imaging of control siRNA cells (Supplementary information, Figure S4A and B). To verify that the observed phenotypes were attributable specifically to disruption of *NUP98* protein levels, and to determine whether the mitotic roles of *NUP98* could be uncoupled, we performed RNAi-resistant *NUP98* rescue experiment by overexpressing GFP-*NUP98* in *NUP98* siRNA cells. Forty-eight hours after transfection of GFP-*NUP98* into *NUP98* siRNA cells, we were able to visualize GFP signals and score the mitotic cells. We found that multipolar spindles/chromosome defects were partially rescued ($n > 300$ mitotic cells) (Figure 1G), indicating that these phenotypes result specifically from alterations in the level of *NUP98*. Together, these results suggest that *NUP98*, working together with *RAE1*[10, 11], is involved in regulating proper chromosome segregation to prevent aneuploidy.

RAE1 interacts with GLEBS domain of N terminal of NUP98 and NUP98-HOXA9 leukemic fusion proteins.

The above depletion experiments prompted us to explore whether exogenously overexpressed NUP98 also altered RAE1 functions. Because the N-termini of NUP98 leukemogenic fusion proteins retain the GLEBS domain for RAE1 interaction [18], we wanted to test whether RAE1 directly influences leukemia formation. We first co-expressed FLAG-RAE1 with NUP98, NUP98-HOXA9 or HOXA9 (Figure 2A) in a cell-free reticulocyte translation system. Consistent with our predictions, NUP98 and the NUP98-HOXA9 fusion, but not HOXA9, interacted directly with RAE1 (Figure 2A). We then performed direct binding assays by loading glutathione-S-transferase (GST), GST-NUP98-N₁₋₅₀₅ or GST-NUP98-C₅₀₆₋₉₂₀ fragments mixed with *in vitro*-translated FLAG-RAE1 proteins. After extensive washing, the bound fraction was analyzed by western blotting to detect FLAG-RAE1. Consistent with a recent report [18], the N-terminal fragment GST-NUP98-N₁₋₅₀₅, but not the C-terminal fragment GST-NUP98-C₅₀₆₋₉₂₀, interacted directly with RAE1 (Figure 2B). GST alone was used as a control and did not bind to RAE1. The N-terminal fragment of NUP98 contains a GLEBS motif for RAE1 binding. To confirm the fine mapping between NUP98_{GLEBS} and RAE1, we expressed FLAG-RAE1 in a cell-free reticulocyte translation system and pulled it down with wild-type (WT) (GST-NUP98 N_{1-505_GLEBS(WT)}) or mutant (GST-NUP98 N_{1-505_GLEBS-(E201K/E202K)}) NUP98 GLEBS domain constructs or GST alone (control). As shown in Figure 2C, RAE1 was specifically pulled down by GST-NUP98 N_{1-505_GLEBS(WT)}. To test for interaction with RAE1 *in vivo*, we further expressed these fragments with GFP tags, GFP-NUP98 N_{1-505_GLEBS(WT)}, or GFP-NUP98 N_{1-505_GLEBS-(E201K/E202K)}, or an empty GFP-vector in HEK 293T cells. As shown in Figure 2D, RAE1 was specifically pulled down by GFP-NUP98 N_{1-505_GLEBS(WT)}, but not

by GFP-NUP98 N_{1-505_GLEBS-(E201K/E202K)} or an empty GFP vector. These data demonstrated that the mutant NUP98 N_{1-505_GLEBS-(E201K/E202K)} did not bind RAE1. The GLEBS ending region is sufficient for RAE1 binding (Figure 2 C and D). These biochemical mapping data also imply that RAE1 binds directly to the ending region of the GLEBS binding site of NUP98, which is present in all NUP98 leukemogenic fusion proteins.

We next examined the sub-cellular localization of the NUP98 and NUP98-HOXA9 proteins together with RAE1 during the cell cycle, by transfecting hemagglutinin (HA)-tagged NUP98 and NUP98-HOXA9 cDNAs into HeLa cells. Lowly expressed transfected proteins with the HA tag were visualized by immunostaining and DAPI staining, immunostaining with or without NUP98 antibody (Supplementary information, Figure S5A and B) or RAE1 antibody (Figure 2E and F). Our findings were in accordance with previous reports that RAE1 was localized on the spindles/kinetochores during metaphase (Figure 2E and F)[11, 12, 22]. Interestingly, we found that during the metaphase-anaphase transition, the leukemogenic fusion protein NUP98-HOXA9 appeared as punctate dots associated with chromatin (Figure 2F, and Supplementary information, Figure S5C), whereas NUP98 was found diffusely throughout the cytoplasm, was not associated with chromatin and was only partially associated with RAE1 (Figure 2E, white arrow). These observations suggest that the NUP98-HOXA9 fusion disturbed the normal NUP98 nuclear rim localization, even with the N-terminal FG repeats intact. We found that the RAE1 immunofluorescence signals were generally weaker in transfected HA-NUP98-HOXA9 cells than in HA-NUP98-transfected cells. However, our HA antibodies could not differentiate clearly between HA-NUP98 and

HA-NUP98-HOXA9.

Expression of exogenous NUP98-HOXA9 robustly reduced RAE1 expression in HeLa, MCF7 and K562 cell lines.

To verify the effect of NUP98 or NUP98-HOXA9 overexpression on RAE1 distribution and expression, we generated visible GFP-tag constructs, GFP-HA-NUP98 and GFP-HA-NUP98-HOXA9, and transfected them into HeLa cells (Figure 3A and B). Strikingly and completely unexpectedly, in triplicate confocal microscopy experiments, quantified using Image J software ($n > 300$ transfected mitotic cells), we found that RAE1 levels were robustly reduced in highly expressing GFP-NUP98-HOXA9 HeLa cells (Figure 3C and H) and the human breast adenocarcinoma cell line, MCF7 (Figure 3D) and more importantly, the leukemia cell line, K562 (Figure 3E) comparing to a much lesser extent in GFP-NUP98 cells (Supplementary information, Figure S6A-C). Both of highly transfected GFP-NUP98-HOXA9 or GFP-NUP98 cells were elevated chromosome defects significantly (Figure 3F and G). Interestingly, we repeatedly observed that some of RAE1 resulted in a punctate distribution on the chromosomes in those GFP-NUP98-HOXA9 cells which was rarely found in GFP-NUP98 chromosome defects cells; and some of NUP98-HOXA9 (indicated as GFP fluorescence signals) were pulled out from chromosomes (Figure 3F and G) compared with low transfected NUP98-HOXA9 localization (Figure 2F). These data indicated that transient altered localization patterns between RAE1 and NUP98-HOXA9 elevated chromosome instability leading to aneuploidy during cell division. Moreover, immunoprecipitation with anti-GFP (Figure 3B) from HeLa and leukemia K562 cell lysates expressing GFP,

GFP-NUP98 or GFP-NUP98-HOXA9 further confirmed the reduction of RAE1 protein (Figure 3H and Supplementary information, Figure S6D). We further quantitated (relative %) the relative RAE1 fluorescence intensity, we found that RAE1 was significantly also reduced ($p < 0.05$) in GFP-NUP98-HOXA9 (Figure 3I) but not in GFP-NUP98-transfected HeLa and MCF7 cells (Supplementary information, Figure S6E). Taken together, these results suggest that RAE1 might be a crucial marker in overexpressed NUP98-HOXA9 leukemogenic fusion cells.

Reduced RAE1 expressions are also found in the spleen of NUP98-HOXA9 transgenic mice and in the bone marrow of NUP98-HOXA9 AML patient

To confirm our cellular observations (Figure 3C-G) and our speculation that the reduction in RAE1 in NUP98-HOXA9 fusions is critical to leukemogenesis, we investigated NUP98-HOXA9-expressing transgenic mice. Consistent with a previous report [25, 26], histological examination of leukemic NUP98-HOXA9 transgenic animals revealed that megakaryocytic cells were frequently found in the spleen; this was seldom observed in WT littermates and non-leukemic NUP98-HOXA9 transgenic mice (Figure 4A). Consistently, we found that RAE1 and endogenous NUP98 expression was reduced in those multinucleated megakaryocytic spleen cells of NUP98-HOXA9 transgenic mice (3 independent transgenic lines), but not in WT mice by immunoblotting, in triplicate experiments. The same membrane was re-probed with β -actin as a loading control (Figure 4B). Interestingly, low RAE1 expression was restricted to the multinucleated megakaryocytic spleen cells that were observed only in NUP98-HOXA9 leukemic transgenic mice by confocal microscopy (Figure 4C and D and Supplementary information, Figure S6F).

To further strengthen our hypothesis that RAE1 is involved in NUP98 fusion-mediated leukemogenesis, we systematically investigated the bone marrow of 52 Chinese AML and MDS patients, representative 6 of them were shown in [Figure 4E](#) (and also [Supplementary information, Table S2](#)). By RT-PCR from bone marrow cells, we identified one AML patient with a NUP98-HOXA9 translocation. Consistent with our results in cellular and rodent models, *RAE1* and endogenous *NUP98* mRNA levels were dramatically reduced in the bone marrow of this NUP98-HOXA9 patient ([Figure 4F and G](#)), but were unaltered in others.

HOXA9 binds to RAE1 promoter region in NUP98HOXA9 mice and other leukemia cell lines

Finally, since NUP98–HOXA9 initiates transformation through HOXA9-mediated DNA binding and transcription, to test whether HOXA9 could bind the RAE1 promoter and modulate its expression, we used GenBank and GenAge [27] databases, mining the RAE1 transcription promoter region. Strikingly, we found that RAE1 contains a HOXA9 consensus sequence, GATTTAT [28, 29] ([Supplementary information, Figure S7A](#)). Because NUP98–HOXA9 initiates transformation through HOXA9-mediated DNA binding and transcription, we tested whether HOXA9 could bind the RAE1 promoter and activate its expression directly. On the basis of ChIP (Chromatin immunoprecipitation) assays from HOXA9, we further demonstrated that the transcription factor HOXA9 also directly participate in the regulation of RAE1 in NUP98-HOXA9 transgenic mice derived cell lines or other leukemia or cancer cell lines ([Supplementary information, Figure S7B](#)). Finally, consistent confirmation from some

of recent microarray analyses revealed that RAE1 gene expression is low in AML patients [30, 31] compared with controls (<http://www.oncomine.org>) [32]. These CHIP assay and proteomic data further show that RAE1 can be regulated by NUP98–HOXA9 and subsequently contribute to leukemogenesis.

Discussion

At first glance, our data showing nucleoporin RAE1 is involved in NUP98-HOXA9 leukemogenesis. RAE1 and NUP98 are components of the NPC facilitating mRNA export during interphase. HOXA9 is a member of the homeobox family, playing a regulatory role in the self-renewal of hematopoiesis [6, 33]. Expression of exogenous NUP98-HOXA9 in murine bone marrow resulted in myeloproliferative disease progressing to AML by 8 months [25, 26], and enhanced stem cell proliferation [34]. The current model of NUP98 leukemogenesis has focused on mis-regulation of transcription due to coupling of DNA binding through the homeodomain to the recruitment of chromatin-modifying co-regulators by the NUP98 FG repeats [7, 13, 15]. This combination of activities leads to upregulation of homeodomain target genes, such as HOXA9 or MEIS. However, there is insufficient direct clinical evidence for this hypothesis [15]. Here we provide an alternative model whereby NUP98 fusion causes chromosome segregation defects during mitosis together with RAE1 ([Supplementary information, Figure S8](#)). The two models are not necessarily mutually exclusive.

We first confirmed the RAE1-NUP98 interaction ([Figure 2A–D](#)) and defined their functional relationship throughout the cell cycle ([Figure 1C and D](#)). Our RNAi NUP98 depletion assays and rescue experiments clearly showed that knockdown of NUP98 remarkably reduced RAE1 activity. Our data suggest that NUP98, working together with RAE1, is involved in regulating proper chromosome segregation to prevent aneuploidy.

We also demonstrated the dramatic differences between NUP98 and NUP98-HOXA9

leukemogenic fusions during mitosis (Figure 2E and F). Endogenous NUP98 was localized diffusely throughout the cells. Remarkably, NUP98-HOXA9 was concentrated at the chromosome arms and kinetochores. It is a recurrent theme in AML that fusion proteins acquire novel intranuclear localizations as well as novel activities [15]. During metaphase, low-level GFP-NUP98-HOXA9 was expressed in a fine punctate pattern concentrated on the chromosome arms and kinetochores. This localization pattern was clearly distinct from that of WT proteins (Figure 2E and F). Besides, NUP98-HOXA9 was not found at the NPC; one possibility is that the N-terminal binding interactions through the nucleoporin repeats of NUP98 act synergistically to generate novel protein targeting and other functions that lead to leukemogenic transformation [7, 13]. Interestingly, NUP98 depletion showed that nuclei/chromatin sizes were generally smaller than those of non-depleted cells (Figure 1C). The size of nucleus is usually proportional to the size of the cell itself [35]. Recent studies indicated that another NUP98 binding partner Karyopherins/importin- α is actively involved[36]. Whether NUP98 directly regulates nuclear size or not need further investigation. Besides, NUP98 might be involved in histone modification in other ways, because NUP98-JARID1A was recently reported to bind specifically to trimethylated histone H3K4 [37, 38]. However, there are no known H3-specific binding sites in either NUP98 or NUP98-HOXA9. Whether NUP98-HOXA9 regulates transcription *via* histone modifications will also require further investigation.

Our study also demonstrates that reduced the expression level of endogenous NUP98 protein in megakaryocytic NUP98-HOXA9 transgenic mice (Figure 4A-D) and *NUP98-HOXA9* mRNA in the bone marrow of an AML patient (Figure 4E-G). Because

of the heterozygous nature of NUP98 translocations in leukemia patients and the lack of detectable fusion protein at the NPC, the NPC in these patients is presumably deficient in NUP98. Such a 30–50% reduction in NUP98 protein levels could seriously affect the normal function of RAE1 and/or NUP98. In addition, Gle2, the yeast homolog of RAE1, and NUP116 (homolog of human NUP98) are required for NPCs with abnormal morphology. Knock-out either one generates pore with a membrane dome that are incompetent of nucleocytoplasmic transport [17, 39]. In fact, our data support this notion (Figures 1 and 3). In particular, in wholly depleted NUP98 cells, RAE1 localization and expression were entirely disrupted and caused serious mitotic errors (Figure 1D and Supplementary information, Figure S4) which enhanced aneuploidy formation. With these detailed *in vitro*, rodent and human clinical data, we proposed a tentative model (negative feedback loop) to explain how RAE1 contributed in NUP98 fusion-mediated leukemogenesis (Supplementary information, Figure S8). We suggest that overexpression of the NUP98 leukemogenic fusion protein (*e.g.*, NUP98-HOXA9) causes a reduction in endogenous NUP98. NUP98 reduction also leads to a disruption in RAE1 localization and function during interphase and cell division (Figure 1 and Supplementary information, Figure S1-4). We found that RAE1 depletion led to aneuploidy (Figure 1D–F and Supplementary information, Figure S3-4) and caused spindle and chromosome segregation defects and the formation of multiple centrosomes, thereby activating leukemogenesis [40-42] (Supplementary information, Figure S3). The kinetics of AML formation is influenced by many other components that will likely modify the effects we reported here for RAE1 and NUP98-HOXA9.

In summary, our cellular findings are in excellent agreement with our rodent and human clinical data on the expression of, and interaction between, RAE1 and NUP98.

These data clearly demonstrate that RAE1 is actively involved in NUP98 fusion-mediated leukemogenesis.

Materials and Methods

Plasmid construction

The plasmid encoding full-length human NUP98, tagged with GFP, was a kind gift from Dr. Nabeel Yaseen (Washington University School of Medicine). Two fragments of NUP98 (N and C) were subcloned by PCR from pcDNA3-NUP98 into pET28a-GST, (pET28a modified to contain a N-terminal GST together with an N-terminal His6 tag).

For the generation of EGFP and HA-tagged NUP98 expression plasmid, a cDNA encoding full length NUP98 tagged with HA were further subclone into pEGFPC2 vector.

The details of expression constructs and cloning primers are listed in [Supplementary information, Table S1A and B](#). All constructs were confirmed by DNA sequencing.

Sequence analyses were performed at the DNA sequencing facility of the Kanazawa University Cancer Research Institute using a PRISM3100-AvantGenetic Analyzer (Applied Biosystems). DNA and protein data bases were searched using the BLAST or BLAT search algorithms at the NCBI.

Mammalian Cell Culture, Transfections, and Synchronization

HeLa, HEK293T, MCF-7, K562, and KG1 cells were obtained from the American Type

Culture Collection (ATCC) and were synchronized in S phase by double thymidine block using 2mM thymidine for mitotic cell collection, if necessary. Cells were transfected with plasmids using Turbofect, following the manufacturer's protocol (Fermentas). The HeLa GFP-H2B or GFP- α -tubulin cell line was generated by transfection of GFP-H2B or GFP- α -tubulin cDNA to HeLa cells respectively; and maintained in G418 (600 μ g/ml). The HeLa GFP-H2B or GFP- α -tubulin cell line was used for analysis of mitotic progression.

RNA interference

siRNA duplexes targeting NUP98 (sc-43535) and control siRNA (sc-37007) were purchased from Santa Cruz Biotechnology. siRNA transfections were performed using Lipofectamine 2000, following the manufacturer's protocol (Invitrogen). HeLa cells were transfected 24 h before the initiation of the first thymidine block and collected or imaged 72 h after transfection. If necessary, transfection efficiency was monitored with Block-iT (Invitrogen).

Antibodies, Immunocytochemistry, and Confocal Microscopy

α -RAE1 and α -NUP98 polyclonal antibody were from Dr. Gunter Blobel (Rockefeller

University). Secondary antibodies were from GE and Molecular Probes. The details of antibody usages and dilutions were listed in [Supplementary information, Table S1C](#).

For immunofluorescence, synchronized HeLa cells were washed in phosphate-buffered saline (PBS) and fixed for 10 min in 4% paraformaldehyde in PBS. Cells were then permeabilized with 0.2% Triton X-100 in PBS for 10 min at room temperature. Samples were mounted onto coverslips with Pro- Long Gold Antifade reagent (Invitrogen) and were examined on a Zeiss LSM5 EXCITER confocal microscope, and all images were acquired using an aplan-Apochromat 63× with a 1.4-N.A. objective or at 100×with a 1.4-N.A. objective.

Immunoprecipitations

For NUP98 immunoprecipitations(IP), $\sim 10^7$ cells were seeded and synchronized as described above. Mitotic HeLa cells were collected, washed with PBS, spun at 400×g for 10 min, and lysed in 1 ml of cold lysis buffer (50 mM Tris-HCl (pH 7.2), 250 mM NaCl, 0.1% NonidetP-40, 2mM EDTA, 10% glycerol) containing 1×protease inhibitor mixture (Roche Applied Science) and 1mM phenylmethylsulfonyl fluoride. Lysates were centrifuged for 30 min at 4 °C at 14,000 × g. The resulting lysate supernatants were precleared with 50 μl of protein A/G bead slurry (Santa Cruz Biotechnology),

mixed with 10 μ l of various antibodies as specified, and incubated for 1 h at 4 °C with rocking. The beads were then washed five times with 500 μ l of lysis buffer. After the last wash, 50 μ l of 1 \times SDS-PAGE blue loading buffer (New England Biolabs) was added to the bead pellet before loading.

Expression of Recombinant Proteins

For expression of NUP98 fragments, Escherichia coli BL21(DE3)-Condon plus cells and pLys cells (Stratagene) were grown at 37 °C to an A600 of 0.6 and induced with 0.5 mM isopropyl- β -D-thiogalactopyranoside at 18 °C for 7 h. The cells were harvested by centrifugation and lysed in buffer containing 50mM Tris-HCl (pH 7.7), 150mM KCl, 0.1% Triton-X100, 1 mM phenylmethylsulfonyl fluoride, and Complete EDTA-free protease inhibitor mixture tablets (Roche Applied Science). The cells were lysed with a cell sonicator (SMT), and the lysate was clarified by centrifugation at 15,000 \times g for 60 min. The proteins containing the GST tag were purified by glutathione affinity (GE Healthcare).

Biochemical “Cell-free” Binding Assays

Proteins were expressed using the Promega TNT coupled transcription/translation

system according to the manufacturer's protocol. Each GST-tagged protein was loaded onto glutathione-agarose beads (GE Healthcare) in lysis buffer (50 mM Tris-HCl (pH 7.7), 150 mM KCl, 0.1% Triton-X100, 1×protease inhibitor mixture) for 1 h at 4 °C. The beads were washed with wash buffer (50 mM Tris-HCl (pH 7.7), 300mM KCl) and incubated with in vitro translated proteins for 2 h at 4 °C. The beads were then washed five times with wash buffer. After the last wash, 1 × SDS-PAGE blue loading buffer was added to the beads before loading.

Time-lapse Microscopy

Time-lapse analysis of histone dynamics during metaphase and anaphase transition in live cells was recorded by GFP-H2B or GFP- α -tubulin stable cell lines. Cells were placed in a microincubation chamber (7136; Corning) on the stage of a Zeiss LSM5 confocal microscope, which was heated to 37 °C and equipped with CO₂ supply (Electric CO₂ Microscope Stage Incubator; OKO Lab). Time-lapse series were generated by collecting photographs every 3 min; the photographs were then converted to 8-bit images and processed by Adobe Photoshop CS2 and Quick-Time software.

Histological Analysis

Mice (12 wks or above) were fixed in 10% Formalin Neutral Buffer solution (Wako).

The spleen tissues were then removed, washed, dehydrated in a graded series of ethanol, and embedded in Paraplast (Oxford Labware). The blocks were cut by using a rotatory microtome (HM355; Rotary Microtome Zeiss) and sectioned serially at 5 μ m thickness by using the same microtome. They were mounted on glass slides, deparafinized, and stained with hematoxylin/eosin solution as described previously [43]. All of the animal protocols used in this study were approved by the Kanazawa University Committee on Animal Welfare.

ChIP assay

The chromatin immunoprecipitation (ChIP) assay was performed using OneDay ChIPTM Kit (Diagenode Inc) according to the manufacturer's instructions with some modifications. Human KG1, K562, HeLa, and NUP98-HOXA9 transgenic mice derived cell lines (NH143 and T2539) (5×10^6) were cross-linked by adding 1% formaldehyde directly to the culture medium for 10 min at 37°C. The cells were then lysed with the lysis buffer supplied in the kit and sonicated at 4°C for five 10-s periods. Approximately 1% of the resulting sample was kept to serve as an input genomic DNA control, and the rest was pre-cleared with salmon sperm DNA-protein A. Cell lysates were incubated with HOXA9 antibody (SC-17155; Santa Cruz Biotechnology) overnight at 4°C with

rotation, followed by a 2h incubation with protein A-agarose for ChIP. HOXA9 in the immunoprecipitate was detected by Western blotting. The precipitated chromatin-HOXA9 complex was washed and eluted, and cross-links were reversed by heating at 65°C for 4 h. The genomic DNA fragments, thus isolated, were purified followed the manufacturer's instructions and amplified by PCR. The PCR products were separated on a 2% agarose gel. The primer sets for PCR were designed to cover the regions of the RAE1 promoter. The primer sequences were 5'-TTGGCCAGACTTGTCTTGAA-3' and 5'-GCCGCTGCAAGTTACTAAGC-3'.

Patients

All healthy adults and patients were diagnosed at West China Hospital, Sichuan University in 2009. All cases were diagnosed with bone marrow aspirates, blood smears, trephine biopsies, flow cytometry and/or cytogenetic analysis. Clinical parameters, hemogram data, and flow cytometry results at the time of diagnosis were reviewed. The diagnosis and classification of AML were based on the criteria established by the WHO. All the samples are collected with the approval of Sichuan University West China Hospital Research Ethics Committee, and written informed consent was obtained from each subject. Patients with antecedent hematologic diseases or therapy-related AML

were excluded.

One patient was the subject of this study. The 56-year old patient was referred to our hospital due to symptoms of ecchymosis and abnormal complete blood count. Physical examination revealed petechial and ecchymosis in skin. The measurements of peripheral blood values were as follows: hemoglobin 100g/L, platelets 23×10^9 /L, and white blood cell count 2.3×10^9 /L. The bone marrow (BM) aspirates were hypercellular, with 69% myeloblasts, 43% of which were strongly positive for myeloperoxidase. Immunophenotypic analysis showed that the blasts were positive for CD34 , HLA-DR, CD13, CD33 , CD117 and CD56. A diagnosis of AML was made according to the World Health Organization criteria. The patient and her family give up any treatments after diagnosis due to economical reasons. For details, please see [Supplementary information, Table S2](#).

Detection of NUP98-HOXA9 fusion transcript.

Total RNAs were extracted from bone marrow cells using Trizol method (Qiagen) according to the manufacturer's instructions. A total of 2 μ g RNA was reverse transcribed at 42°C for 1 h in 20 μ l reaction mixture containing Moloney murine leukemia virus reverse transcriptase kit (TAKARA). Serially twofold diluted cDNA

products were amplified for glyceraldehyde-3-phosphate dehydrogenase (GAPDH) using a specific set of primers using 25 cycles consisting of following reaction conditions: 94°C for 30 s, 58°C for 30 s and 72°C for 1 min in a 25- μ l of reaction mixture containing Taq polymerase (Roche) to evaluate the quantity of the transcribed cDNA. Equal quantities of cDNA products were then amplified for the indicated genes using the specific sets of primers (Supplementary information, Table S1B) with 35 cycles consisting of following conditions: 94 °C for 30 s, 55 °C for 1 min and 72 °C for 1 min. The resultant PCR products were fractionated on 1.5% agarose gel and visualized by ethidium bromide staining under ultraviolet light trans-illumination. The band intensities were measured using National Institutes of Health Image analysis software, version 1.62, and the ratios to GAPDH were calculated on the assumption that the ratios of the normal were set at 1.0.

Statistical Analyses

All data represent the average from at least three independent experiments, with at least 100 cells counted per experiment. Significant were calculated by Student t-test. Differences were considered significant when p was < 0.05 . Error bars represent mean \pm S.D. of three different experiments.

Acknowledgments

We thank Dr. Nabeel Yaseen for the NUP98 plasmids. NUP98-HOXA9 transgenic mice were provided by the RIKEN BRC through the National Bio-Resource Project of the MEXT. We thank Kenji Anezaki for technical assistant. We are very grateful to Dr. Günter Blobel in his lab this project was initiated. This work was supported by the Program for Improvement of the Research Environment for Young Researchers from the Special Coordination Funds for Promoting Science and Technology (SCF), Grants-in-Aid for Scientific Research on Innovative Areas and Young Scientists from MEXT Japan, and also by grants from the Asahi Glass Foundation, the Mochida Memorial foundation, the Suzuken Memorial Foundation, the Kowa Life Science foundation, the Takeda Science Foundation, the Astellas Foundation and the Novartis Foundation (Japan) to RW.

Figure legends

Figure 1. Knockdown NUP98 abolished RAE1 localization and expression.

(A) Effects of NUP98 depletion on protein levels of NUP98-associated proteins. Lysates of control siRNA and lysates of NUP98 siRNAs (NUP98 RNAi) in HeLa cells. 72 h after transfection were analyzed by immunoblotting (IB) with the indicated antibodies. The same membrane was stripped and re-probed with anti- α -tubulin (as loading control). Numbers indicate molecular masses markers in kilodaltons. (B) Quantitation (relative %) of relative expression of NUP98, RAE1 and HDAC1 in control siRNA and NUP98 siRNA-transfected (72hr) HeLa cells. Mean values \pm S.D. (error bars) are

shown. (C) Representative images of interphase HeLa cells, transfected with either control siRNA duplex or NUP98 siRNA. 72 h after transfection, cells were stained with anti-NUP98 antibody (green) or RAE1 antibody (red) and analyzed by confocal laser microscopy respectively. Chromatin was stained with DAPI (blue). Scale bars, 10 μ m. Normally, NUP98 displayed nuclear rim staining. During interphase, NUP98 was dramatically reduced at the nuclear rim signals, 72 h after transfection with NUP98-specific siRNAs. Nuclei size was relatively smaller in NUP98 depleted cells. White circle indicates a remained non-depleted NUP98 cell. (D) Pictorial presentation of various mitotic errors of mitotic HeLa cells, transfected with siRNA duplex against NUP98. 72 h after transfection, cells were stained with anti-NUP98 antibody (green) or RAE1 antibody (red) and analyzed by confocal laser microscopy. Chromatin was stained with DAPI (blue). Scale bars, 10 μ m. Mitotic NUP98 was dramatically reduced at the kinetochores, 72 h after transfection with NUP98-specific siRNAs. White arrows indicate RAE1 kinetochore and spindle staining in a remained non-depleted NUP98 cell. White circle indicates typical chromosomes missegregation NUP98 depleted cells, RAE1 expression was also reduced in those mitotic NUP98 depleted cells. (E) Quantification of mitotic errors in control siRNA and NUP98 siRNA assays. Graph indicate the percentage of cells with abnormal spindles (counting from tubulin and/or pericentrin antibodies (refer to [Supplementary information, Figure S3](#)). Column, mean (n=3); Mean values \pm S.D. (error bars) are shown. (F) Quantification of mitotic errors in control siRNA and NUP98 siRNA assays. Graph indicate the percentage of cells with abnormal monopolar (blue) and multipolar (brown) spindles (counting from tubulin and/or pericentrin antibodies (refer to [Supplementary information, Figure S3](#)). Column, mean (n=3); Mean values \pm S.D. (error bars) are shown. (G) Quantification of mitotic

errors in control siRNA, NUP98 siRNA and cotransfection with NUP98 rescue assays. Mitotic HeLa cells were scored for abnormal spindles. The graph represents means of three independent experiments in which 100 mitotic cells were scored at each time. Graph indicates the percentage of cells with abnormal spindles (counting from tubulin and/or pericentrin antibodies (refer to [Supplementary information, Figure S3](#)). Column, mean (n=3); Mean values \pm S.D. (error bars) are shown.

Figure 2. RAE1 interacts with GLEBS domain of N terminal of NUP98 and also NUP98-HOXA9 leukemic fusion proteins. (A) Autoradiograph of [³⁵S] methionine-labeled FLAG-RAE1 and NUP98-HOXA9, and NUP98-HOXA9 coexpressed *in vitro*, affinity-purified with FLAG beads, and separated by SDS/PAGE respectively. (B) RAE1 (untagged) expressed *in vitro*, affinity-purified together with recombinant proteins of GST, GST-NUP98-N₁₋₅₀₅, and GST-NUP98-C₅₀₆₋₉₂₀, and separated by SDS-PAGE. Numbers on the bottom refer to amino acids; all fragments are continuous (e.g. NUP98-N ends at amino acid 505, and NUP98-C starts at amino acid 506). RAE1 was prepared from TNT Quick-Coupled Transcription/translation system (Promega) together with TranscendTM Biotin-Lysyl-tRNA (Promega). Detection was done by streptavidin horseradish peroxidase (HRP) (1:4,000). (C) Examination of the interaction between RAE1 and GST-NUP98 GLEBS mutants. GST pull down assays indicated that the GLEBS is sufficient for RAE1 binding. A double mutant in GLEBS, E201K/E202K, abolishes the RAE1-NUP98^{GLEBS} interaction. (D) *In vivo* pull down assays of GFP-tagged NUP98 fusions, GFP-NUP98 N_{1-505_GLEBS(WT)}, or GFP-NUP98 N_{1-505_GLEBS-(E201K/E202K)} and an empty GFP-vector in HEK 293T cells, followed by protein A/G beads-crosslinked anti-GFP IP and immunoblotting with anti-Rae1 and

anti-GFP. **(E, F)** Representative images of mitotic HeLa cells transfected with plasmids overexpressing HA-NUP98 and HA-NUP98-HOXA9. 48 h after transfection, cells were fixed, stained anti-HA (green) and anti-RAE1 (red) antibodies for immunofluorescence visualization and examined by confocal microscopy. Chromatin was stained with DAPI (blue). Scale bars, 5 μ m. White circles indicate different localization pattern between NUP98 and NUP98-HOXA9. White arrows indicate RAE1 spindle localization during metaphase.

Figure 3. Expression of exogenous NUP98-HOXA9 robustly reduced RAE1 expression in HeLa and MCF7 cell lines. **(A)** Schematic of the NUP98 and NUP98-HOXA9 expression plasmids with visible GFP tags. Numbers on the left refer to amino acids. **(B)** HeLa cells were transfected with a GFP-NUP98 or GFP-NUP98-HOXA9 expression plasmid. After 48 h, the cells were lysed and immunoprecipitation with an anti-GFP antibody and analyzed by immunoblotting with an anti-GFP antibody. Asterisks indicate the GFP fusion proteins. **(C-E)** Representative images of C) HeLa cells, D) MCF7 cells and E) K562 cells transfected with plasmids overexpressing GFP-NUP98-HOXA9. 48 h after transfection, cells were fixed, stained with anti-RAE1 antibodies (red in overlay; GFP is green), and analyzed by confocal laser microscopy. Chromatin was stained with DAPI (blue). Scale bars, 10 μ m. **(F-G)** Representative images of mitotic HeLa cells transfected with plasmids overexpressing F) GFP-NUP98-HOXA9 and G) GFP-NUP98 respectively. 48 h after transfection, cells were fixed, stained with anti-RAE1 antibodies (red in overlay; GFP is green), and analyzed by confocal laser microscopy. Chromatin was stained with DAPI (blue). Scale bars, 5 μ m. Some of RAE1 located in a punctate distribution on the

chromosomes in those highly expressed GFP-NUP98-HOXA9 cells (F) which was rarely found in highly expressed GFP-NUP98 chromosome defects cells (G). (H) Immunoprecipitates (IP) from mitotic HeLa cell and K562 cell (Supplementary information, Figure S6D) extracts (prepared same as in Figure 2G) with anti-GFP antibody was analyzed by SDS-PAGE, followed by immunoblotting with RAE1 antibody. (I) Quantitation (relative %) of relative RAE1 fluorescence intensity in GFP, GFP-NUP98 GFP-NUP98-HOXA9 and GFP-HOXA9-transfected HeLa cells. Values are based on three independent experiments, counting 80 transfected cells in each experiment. Mean values \pm S.D. (error bars) are shown.

Figure 4. Reduced RAE1 expressions are found in the megakaryotic spleen of NUP98-HOXA9 transgenic mice and in the bone marrows of NUP98-HOXA9 AML patient. (A) Haematoxylin/erosin staining of spleen tissue from NUP98-HOXA9 transgenic mice and its wild type (WT) littermate. Multinucleated spleen cells (indicates as black arrows) are often found in NUP98-HOXA9 transgenic mice but not its WT littermates. (B) RAE1 and endogeneous NUP98 (antibody only recognizes C-terminal of NUP98) immunoblot of WT and NUP98-HOXA9 transgenic mice spleen. The same membrane was stripped and reprobed with anti- β -actin (as loading control). (C) RAE1 expression is reduced in NUP98-HOXA9 mice but not in WT. Representative immunostaining images of NUP98-HOXA9 transgenic mice and its WT littermate.

Spleen cells were fixed, stained with anti-RAE1 antibodies (green) and mb414 (red), and analyzed by confocal laser microscopy. Chromatin was stained with DAPI (blue). Scale bars, 10 μ m. **(D)** RAE1 expression is robustly reduced in NUP98-HOXA9 mice megakaryotic spleen cells. Representative immunostaining images of NUP98-HOXA9 transgenic mice and its WT littermate. Spleen cells were fixed, stained with anti-RAE1 antibodies (green) and mb414 (red), and analyzed by confocal laser microscopy. Chromatin was stained with DAPI (blue). Scale bars, 10 μ m. White arrow indicates RAE1 reduction compared with WT spleen cells. **(E)** Schematic diagram of NUP98 endogenous proteins and deduced chimeric protein after chromosomal translocation, and sequence of NUP98-HOXA9 fusion transcription junction. Horizontal arrows indicate the RT-PCR primers. **(F)** Reverse transcription-polymerase chain reaction (RT-PCR) analysis of sequential bone marrow samples taken from the patient's bone marrow. Lane 1-2, RT-PCR products of non-leukemia patients; Lane 3-4 RT-PCR products of in AML patients ; Lane 5-6 RT-PCR product of MDS patients; Lane7, RT-PCR products of in AML patient; Lane 8, RT-PCR product of the AML patient with t(7;11) described. The 537 bp NUP98-HOXA9 fusion product was detected in AML patient (Lane8). **(G)** Quantitation (mean values of relative RAE1 intensity) of mRNA expression of RAE1 in patients bone marrow cells. Values are based on three

independent experiments.

References

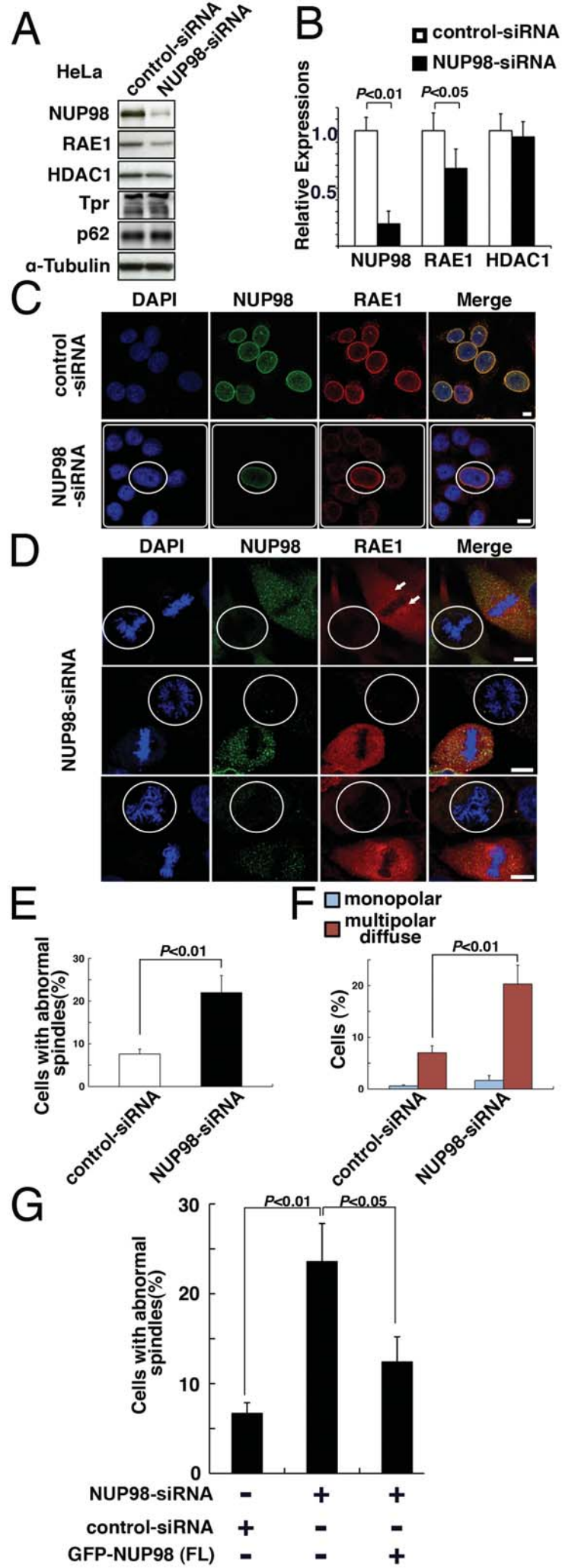
1. Strambio-De-Castillia C, Niepel M, Rout MP. The nuclear pore complex: bridging nuclear transport and gene regulation. *Nat Rev Mol Cell Biol* 2010; 11:490-501.
2. Funasaka T, Wong RW. The role of nuclear pore complex in tumor microenvironment and metastasis. *Cancer Metastasis Rev*.
3. Nakano H, Wang W, Hashizume C, Funasaka T, Sato H, Wong RW. Unexpected role of nucleoporins in coordination of cell cycle progression. *Cell Cycle*; 10:425-33.
4. Guttinger S, Laurell E, Kutay U. Orchestrating nuclear envelope disassembly and reassembly during mitosis. *Nat Rev Mol Cell Biol* 2009; 10:178-91.
5. Tran EJ, Wentz SR. Dynamic nuclear pore complexes: life on the edge. *Cell* 2006; 125:1041-53.
6. Moore MA, Chung KY, Plasilova M, Schuringa JJ, Shieh JH, Zhou P, Morrone G. NUP98 dysregulation in myeloid leukemogenesis. *Ann N Y Acad Sci* 2007; 1106:114-42.
7. Xu S, Powers MA. Nup98-homeodomain fusions interact with endogenous Nup98 during interphase and localize to kinetochores and chromosome arms during mitosis. *Mol Biol Cell* 2010; 21:1585-96.
8. Moore MA. A cancer fate in the hands of a samurai. *Nat Med* 2010; 16:963-5.
9. Pritchard CE, Fornerod M, Kasper LH, van Deursen JM. RAE1 is a shuttling mRNA export factor that binds to a GLEBS-like NUP98 motif at the nuclear pore complex through multiple domains. *J Cell Biol* 1999; 145:237-54.
10. Wong RW. Interaction between Rae1 and cohesin subunit SMC1 is required for proper spindle formation. *Cell Cycle* 2010; 9:198-200.
11. Wong RW, Blobel G. Cohesin subunit SMC1 associates with mitotic microtubules at the spindle pole. *Proc Natl Acad Sci U S A* 2008; 105:15441-5.
12. Wong RW, Blobel G, Coutavas E. Rae1 interaction with NuMA is required for bipolar spindle formation. *Proc Natl Acad Sci U S A* 2006; 103:19783-7.
13. Xu S, Powers MA. Nuclear pore proteins and cancer. *Semin Cell Dev Biol* 2009; 20:620-30.
14. Nakamura T, Largaespada DA, Lee MP, Johnson LA, Ohyashiki K, Toyama K, Chen SJ, Willman CL, Chen IM, Feinberg AP, Jenkins NA, Copeland NG, Shaughnessy JD, Jr. Fusion of the nucleoporin gene NUP98 to HOXA9 by the chromosome translocation t(7;11)(p15;p15) in human myeloid leukaemia. *Nat Genet* 1996; 12:154-8.
15. Kohler A, Hurt E. Gene regulation by nucleoporins and links to cancer. *Mol Cell* 2010; 38:6-15.

16. Nakamura T. NUP98 fusion in human leukemia: dysregulation of the nuclear pore and homeodomain proteins. *Int J Hematol* 2005; 82:21-7.
17. Bailer SM, Siniossoglou S, Podtelejnikov A, Hellwig A, Mann M, Hurt E. Nup116p and nup100p are interchangeable through a conserved motif which constitutes a docking site for the mRNA transport factor gle2p. *EMBO J* 1998; 17:1107-19.
18. Ren Y, Seo HS, Blobel G, Hoelz A. Structural and functional analysis of the interaction between the nucleoporin Nup98 and the mRNA export factor Rae1. *Proc Natl Acad Sci U S A* 2010; 107:10406-11.
19. Kao J, Salari K, Bocanegra M, Choi YL, Girard L, Gandhi J, Kwei KA, Hernandez-Boussard T, Wang P, Gazdar AF, Minna JD, Pollack JR. Molecular profiling of breast cancer cell lines defines relevant tumor models and provides a resource for cancer gene discovery. *PLoS One* 2009; 4:e6146.
20. Chin K, DeVries S, Fridlyand J, Spellman PT, Roydasgupta R, Kuo WL, Lapuk A, Neve RM, Qian Z, Ryder T, Chen F, Feiler H, Tokuyasu T, Kingsley C, Dairkee S, Meng Z, Chew K, Pinkel D, Jain A, Ljung BM, Esserman L, Albertson DG, Waldman FM, Gray JW. Genomic and transcriptional aberrations linked to breast cancer pathophysiologies. *Cancer Cell* 2006; 10:529-41.
21. Lu Y, Lemon W, Liu PY, Yi Y, Morrison C, Yang P, Sun Z, Szoke J, Gerald WL, Watson M, Govindan R, You M. A gene expression signature predicts survival of patients with stage I non-small cell lung cancer. *PLoS Med* 2006; 3:e467.
22. Blower MD, Nachury M, Heald R, Weis K. A Rae1-containing ribonucleoprotein complex is required for mitotic spindle assembly. *Cell* 2005; 121:223-34.
23. Stegmeier F, Rape M, Draviam VM, Nalepa G, Sowa ME, Ang XL, McDonald ER, 3rd, Li MZ, Hannon GJ, Sorger PK, Kirschner MW, Harper JW, Elledge SJ. Anaphase initiation is regulated by antagonistic ubiquitination and deubiquitination activities. *Nature* 2007; 446:876-81.
24. Ohsugi M, Adachi K, Horai R, Kakuta S, Sudo K, Kotaki H, Tokai-Nishizumi N, Sagara H, Iwakura Y, Yamamoto T. Kid-mediated chromosome compaction ensures proper nuclear envelope formation. *Cell* 2008; 132:771-82.
25. Iwasaki M, Kuwata T, Yamazaki Y, Jenkins NA, Copeland NG, Osato M, Ito Y, Kroon E, Sauvageau G, Nakamura T. Identification of cooperative genes for NUP98-HOXA9 in myeloid leukemogenesis using a mouse model. *Blood* 2005; 105:784-93.
26. Kroon E, Thorsteinsdottir U, Mayotte N, Nakamura T, Sauvageau G. NUP98-HOXA9 expression in hemopoietic stem cells induces chronic and acute myeloid leukemias in mice. *EMBO J* 2001; 20:350-61.
27. de Magalhaes JP, Budovsky A, Lehmann G, Costa J, Li Y, Fraifeld V, Church GM. The Human Ageing Genomic Resources: online databases and tools for biogerontologists. *Aging Cell* 2009; 8:65-72.
28. Bandyopadhyay S, Ashraf MZ, Daher P, Howe PH, DiCorleto PE. HOXA9 participates in the transcriptional activation of E-selectin in endothelial cells. *Mol Cell Biol* 2007; 27:4207-16.

29. Shen WF, Rozenfeld S, Kwong A, Kom ves LG, Lawrence HJ, Largman C. HOXA9 forms triple complexes with PBX2 and MEIS1 in myeloid cells. *Mol Cell Biol* 1999; 19:3051-61.
30. Golub TR, Slonim DK, Tamayo P, Huard C, Gaasenbeek M, Mesirov JP, Coller H, Loh ML, Downing JR, Caligiuri MA, Bloomfield CD, Lander ES. Molecular classification of cancer: class discovery and class prediction by gene expression monitoring. *Science* 1999; 286:531-7.
31. Bullinger L, Dohner K, Bair E, Frohling S, Schlenk RF, Tibshirani R, Dohner H, Pollack JR. Use of gene-expression profiling to identify prognostic subclasses in adult acute myeloid leukemia. *N Engl J Med* 2004; 350:1605-16.
32. Rhodes DR, Kalyana-Sundaram S, Mahavisno V, Varambally R, Yu J, Briggs BB, Barrette TR, Anstet MJ, Kincead-Beal C, Kulkarni P, Varambally S, Ghosh D, Chinnaiyan AM. Oncomine 3.0: genes, pathways, and networks in a collection of 18,000 cancer gene expression profiles. *Neoplasia* 2007; 9:166-80.
33. Aoki T, Miyamoto T, Yoshida S, Yamamoto A, Yamauchi T, Yoshimoto G, Mori Y, Kamezaki K, Iwasaki H, Takenaka K, Harada N, Nagafuji K, Teshima T, Akashi K. Additional acquisition of t(1;21)(p32;q22) in a patient relapsing with acute myelogenous leukemia with NUP98-HOXA9. *Int J Hematol* 2008; 88:571-4.
34. Chung KY, Morrone G, Schuringa JJ, Plasilova M, Shieh JH, Zhang Y, Zhou P, Moore MA. Enforced expression of NUP98-HOXA9 in human CD34(+) cells enhances stem cell proliferation. *Cancer Res* 2006; 66:11781-91.
35. Cohen-Fix O. Cell biology: Import and nuclear size. *Nature* 2010; 468:513-6.
36. Levy DL, Heald R. Nuclear size is regulated by importin alpha and Ntf2 in *Xenopus*. *Cell* 2010; 143:288-98.
37. van Zutven LJ, Onen E, Velthuisen SC, van Drunen E, von Bergh AR, van den Heuvel-Eibrink MM, Veronese A, Mecucci C, Negrini M, de Greef GE, Beverloo HB. Identification of NUP98 abnormalities in acute leukemia: JARID1A (12p13) as a new partner gene. *Genes Chromosomes Cancer* 2006; 45:437-46.
38. Wang GG, Song J, Wang Z, Dormann HL, Casadio F, Li H, Luo JL, Patel DJ, Allis CD. Haematopoietic malignancies caused by dysregulation of a chromatin-binding PHD finger. *Nature* 2009; 459:847-51.
39. Strawn LA, Shen T, Wentz SR. The GLFG regions of Nup116p and Nup100p serve as binding sites for both Kap95p and Mex67p at the nuclear pore complex. *J Biol Chem* 2001; 276:6445-52.
40. Falini B. Acute Myeloid Leukemia with Mutated Nucleophosmin (NPM1): Molecular, Pathological, and Clinical Features. *Cancer Treat Res* 2009; 145:149-68.
41. Neben K, Giesecke C, Schweizer S, Ho AD, Kramer A. Centrosome aberrations in acute myeloid leukemia are correlated with cytogenetic risk profile. *Blood* 2003; 101:289-91.
42. Neben K, Tews B, Wrobel G, Hahn M, Kokocinski F, Giesecke C, Krause U, Ho AD, Kramer A,

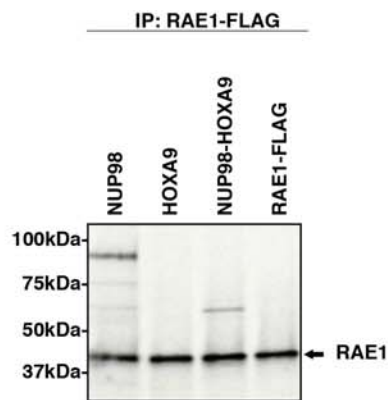
Lichter P. Gene expression patterns in acute myeloid leukemia correlate with centrosome aberrations and numerical chromosome changes. *Oncogene* 2004; 23:2379-84.

43. Wong RW, Setou M, Teng J, Takei Y, Hirokawa N. Overexpression of motor protein KIF17 enhances spatial and working memory in transgenic mice. *Proc Natl Acad Sci U S A* 2002; 99:14500-5.

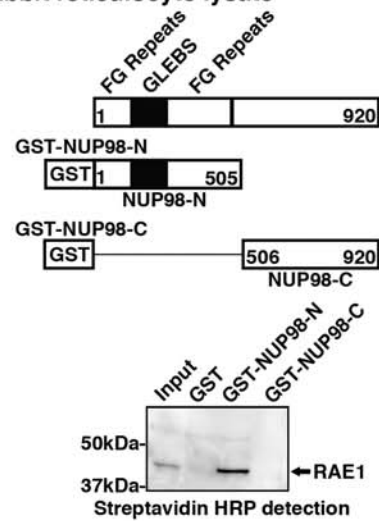


Funasaka_Fig. 1.

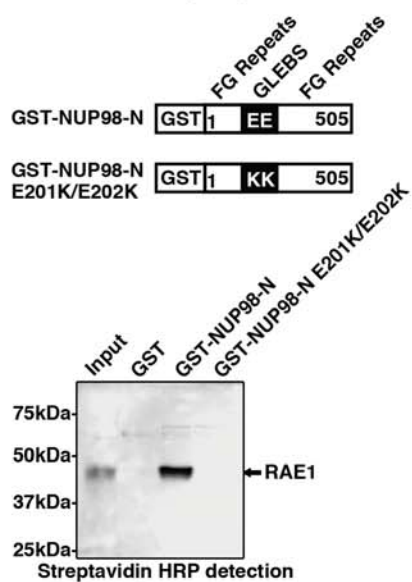
A Rabbit reticulocyte lysate



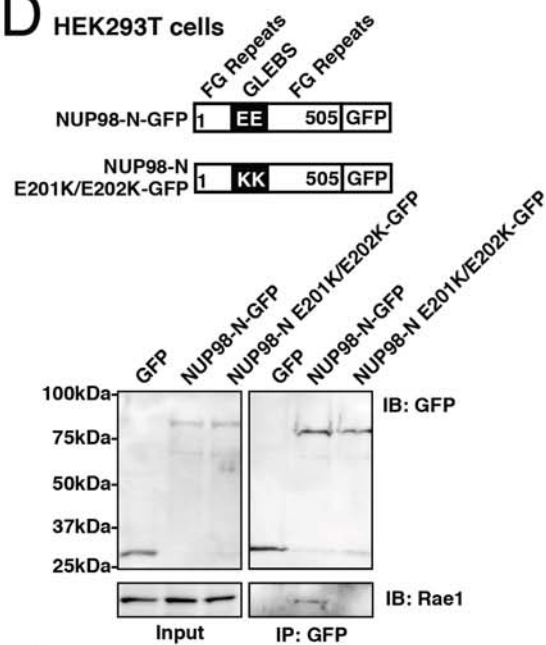
B Rabbit reticulocyte lysate



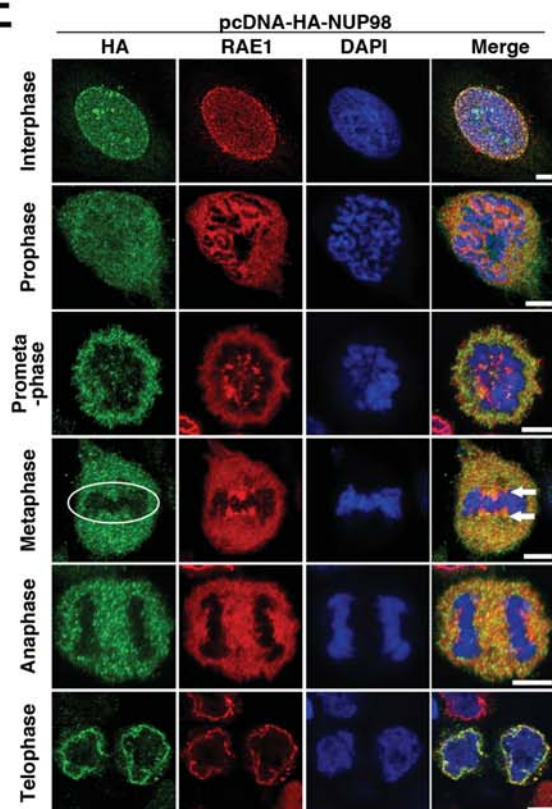
C Rabbit reticulocyte lysate



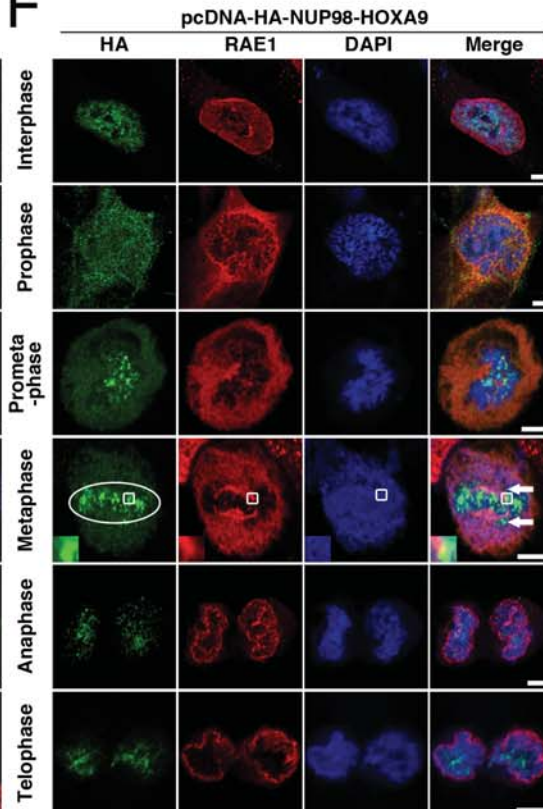
D HEK293T cells

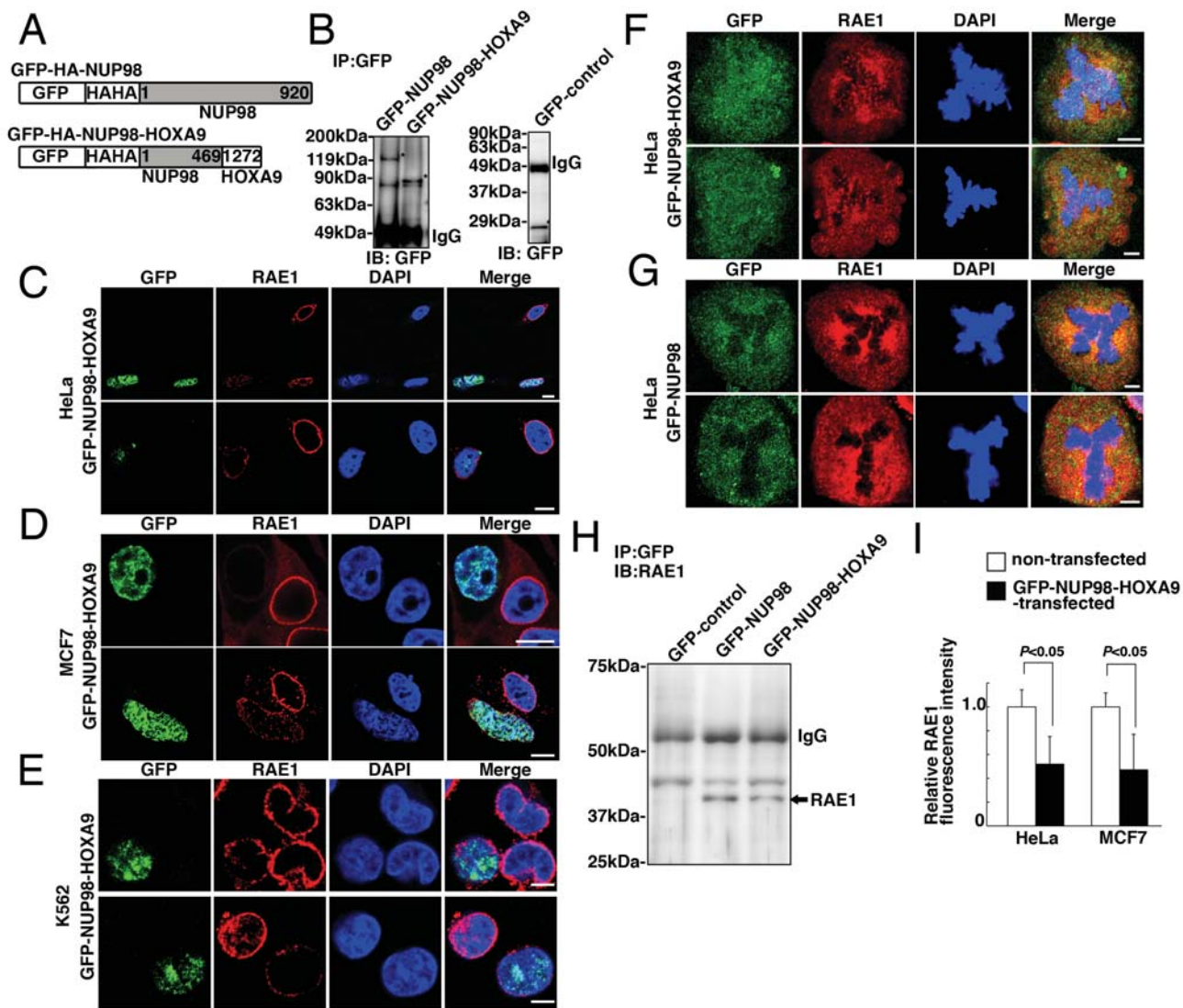


E



F





Funasaka_Fig. 3.

